small NANO MICRO

Cancer Therapy

Mitochondria-Targeting Photoacoustic Therapy Using Single-Walled Carbon Nanotubes

*Feifan Zhou, Shengnan Wu, Yi Yuan, Wei R. Chen, and Da Xing**

In vitro photoacoustic therapy using modified single-walled carbon nanotubes (SWNTs) as "bomb" agents is a newly reported approach for cancer. Herein, a mitochondria-targeting photoacoustic modality using unmodified SWNTs and its in vitro and in vivo antitumor effect are reported. Unmodified SWNTs can be taken up into cancer cells due to a higher mitochondrial transmembrane potential in cancerous cells than normal cells. Under the irradiation of a 1064 nm pulse laser, 79.4% of cancer cells with intracellular SWNTs die within 20 s, while 82.3% of normal cells without SWNTs remain alive. This modality kills cancer cells mainly by triggering cell apoptosis that initiates from mitochondrial damage, through the depolarization of mitochondria and the subsequent release of cytochrome c after photoacoustic therapy. It is very effective in suppressing tumor growth by selectively destroying tumor tissue without causing epidermis injury. Taken together, these discoveries provide a new method using mitochondria-localized SWNTs as photoacoustic transducers for cancer treatment.

1. Introduction

Single-walled carbon nanotubes (SWNTs) exhibit many unique intrinsic photophysical properties and have been intensively explored for biological and biomedical applications in the past several years. One intrinsic property of SWNTs is their strong optical absorbance in the near-infrared (NIR) region.[1,2] Since biological tissues are relatively transparent to the light of the NIR region,[3,4] such a unique property makes SWNTs selective photothermal transducers with a large absorption cross section and highly efficient light-to-heat conversion.[2,5,6] Recent findings on the ignition of SWNTs exposed to a pulsed light source attracted much interest in the photoacoustic properties of nanotubes.[7–10] Because of the photothermal and photoacoustic transduction effects, SWNTs have been used in the past as photothermal agents for killing cancer cells by enhancing thermal destruction of tumor cells under NIR continuous laser irradiation,[2,5,6] and also as contrast agents for cancer imaging by enhancing the photoacoustic contrast of target tumors during pulse laser irradiation.[11–15] Moreover, a novel photoacoustic technique for targeted cancer destruction by the large photoacoustic effect of SWNTs was developed.[10,16]

The ideal treatment modality for cancer should achieve tumor target destruction with local intervention through a minimally invasive technique. It is generally considered that mitochondria are promising therapeutic targets in cancer because of their dominant role in cell apoptosis.[17,18] Mitochondrial outer membrane permeabilization (MOMP)

Dr. F. Zhou,[+] Dr. S. Wu,[+] Dr. Y. Yuan,
Prof. W. R. Chen, Prof. D. Xing
MOE Key Laboratory of Laser Life Science &
Institute of Laser Life Science
College of Biophotonics
South China Normal University
Guangzhou 510631, China
E-mail: xingda@scnu.edu.cn
Dr. F. Zhou,[+] Dr. S. Wu, Prof. D. Xing
Joint Laboratory of Laser Oncology with Cancer
Center of Sun Yat-sen University
South China Normal University
Guangzhou 510631, China
Prof. W. R. Chen
Biomedical Engineering Program
Department of Engineering and Physics
College of Mathematics and Science
University of Central Oklahoma
Edmond, OK 73034, USA
[+] F.Z. and S.W. contributed equally to this work.

DOI: 10.1002/smll.201101892

appears to represent a point of no return for cell death. MOMP can typically lead to cell death by triggering a progressive decline in mitochondrial function.[19,20] Mitochondria in cancer cells are in general more susceptible to perturbations than in normal cells because of their structural and functional differences, and extensive metabolic reprogramming compared with their normal counterparts.[21,22] Therefore, mitochondria-targeted therapies are promising in selectively treating tumors without causing, or at least minimizing, damage to surrounding normal tissue.[23]

Previously, we used SWNTs selectively accumulated in mitochondria as photothermal transducers to destroy cancer cells using a continuous-wave 980 nm laser.[24,25] Herein, we develop a mitochondria-targeting therapy using the photoacoustic transducer property of SWNTs and a NIR pulse laser. We investigate in vitro and in vivo antitumor effects using this mitochondria-targeting photoacoustic therapy.

2. Results

2.1. Photoacoustic Effect of SWNTs in the NIR Spectral Region

CoMoCAT SWNTs functionalized with phospholipid–polyethylene glycol with a terminal amine group (PL-PEG-NH_2) were used in this study. The Vis–NIR absorption spectra of SWNT-PEG solution exhibited a strong band at approximately 1016 nm, significantly higher than that of PEG solution in the same spectral region (**Figure 1**Aa). The absorbance of the SWNT-PEG solution depended linearly on its concentration at a wavelength of 1064 nm, as shown in Figure 1Ab. Raman spectroscopy of SWNT-PEG solution exhibited a strong resonance shift at approximately 1580 cm^{-1} (G band; Figure 1Ac). Moreover, the solution of SWNT-PEG remained stable for more than 2 weeks at room temperature without any visible aggregation, which is probably attributable to the noncovalent interaction between PL-PEG and SWNTs.

The photoacoustic signal could be generated in SWNT solution by irradiation with a 1064 nm pulse laser (Figure 1Ba). The intensity of the photoacoustic signal depended on the concentration of SWNTs and energy of the laser (Figure 1Bb and Bc). To evaluate the thermal effects of the SWNT solution during the 1064 nm pulse laser irradiation, an infrared thermal camera was used to measure the temperature in the solution. As shown in Figure 1Bd, irradiation with 17.5 mJ energy caused a temperature increase of 6 °C in the SWNT solution (200 μg mL^{-1}), whereas the temperature increase was almost negligible in the SWNT solution with a concentration of 50 μg mL^{-1} (Figure 1Bd).

2.2. Photoacoustic Effect on Mitochondria Targeted with SWNTs

Our previous work showed that SWNTs were mainly localized in mitochondria of both tumor cells and normal cells.[24] Here, we further confirm the mitochondrial localization of SWNTs in EMT6 cells. Cells expressing cyan fluorescent protein (CFP)-lamp (to label lysosome) were stained with

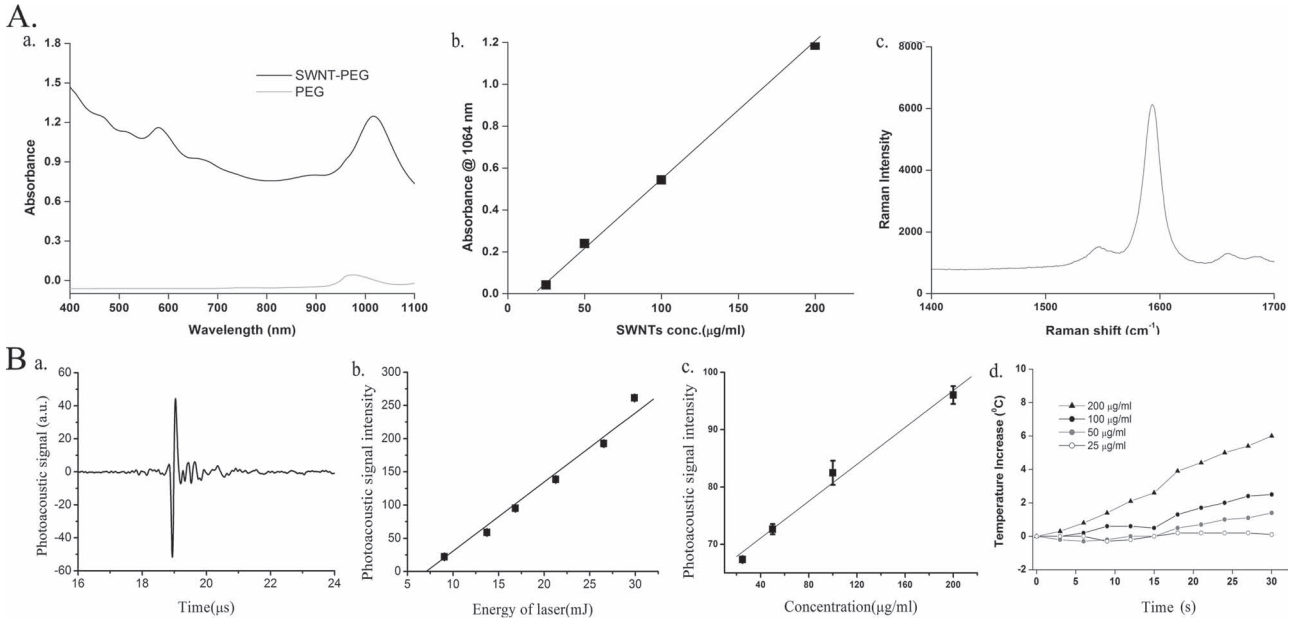

Figure 1. Photoacoustic signals of SWNTs in the NIR spectral region. A) Absorption and Raman spectra of PL-PEG-functionalized SWNTs. a) Vis–NIR absorption spectra of the SWNT-PEG solution and PEG solution. The two well-resolved absorption peaks indicate that the electronic energy states of individual PEG-SWNTs are well maintained after PEGylation. b) Absorbance of SWNT solutions of different concentrations at 1064 nm. The solid line is a linear fit. c) Raman spectrum of SWNT solution. The band is a characteristic feature of SWNTs. B) Photoacoustic signal of SWNTs. a) Photoacoustic signal of SWNT solution at 1064 nm. b,c) Peak intensity of photoacoustic signal versus energy of the laser at 1064 nm (b) or the concentration of the SWNT solution (c). The solid line is a linear fit. d) Temperature of the SWNT solution during irradiation by a pulse laser (1064 nm, 17.5 mJ) for 30 s at room temperature.

small NANO MICRO

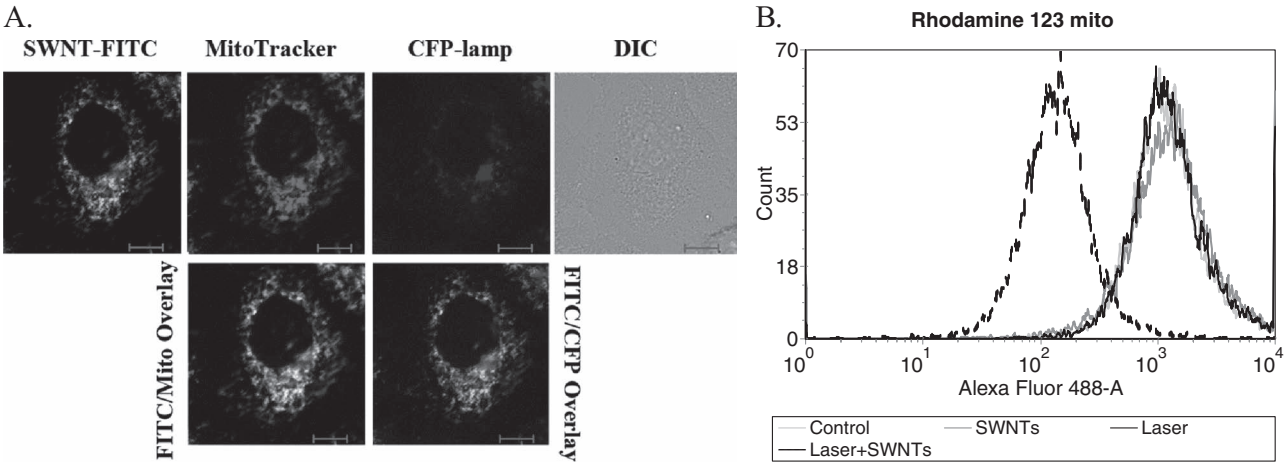

Figure 2. Photoacoustic destruction of mitochondria targeted with SWNTs. A) Mitochondrial localization of SWNTs. Cells expressing CFP-lamp and stained with MitoTracker Red were incubated with SWNT-PEG-FITC for 30 min. Confocal images of the cells show that the SWNT is mainly localized in mitochondria but not in lysosome. DIC=differential interference contrast. B) Change of $\Delta\Psi$m under pulse laser irradiation with SWNTs taken up ex vitro. Mitochondria separated from living cells were stained with Rh123 and incubated with SWNTs (10 μg mL^{-1}) for 30 min before irradiation by a pulse laser (17.5 mJ for 20 s), then subjected to FACS analysis. The decrease in Rh123 signal represents the decline of $\Delta\Psi$m. All the data are representative of four independent experiments.

MitoTracker Deeper Red 633 (MitoTracker Red, to label mitochondria) and then incubated with SWNT-PEG-fluorescein isothiocyanate (FITC) for 30 min. The fluorescence emission of SWNT-PEG-FITC coincided with that of MitoTracker Red (**Figure 2**A), thereby indicating mitochondrial localization of SWNTs.

To test whether the photoacoustic effect of SWNTs could cause mitochondrial damage, we performed an ex vitro experiment with isolated mitochondria. Mitochondria were separated from EMT6 cells, stained with rhodamine 123 (Rh123) dye, and incubated with SWNTs (10 μg mL^{-1}) for 30 min before 1064 nm pulse laser irradiation (17.5 mJ, 20 s). Then the changes in Rh123 fluorescence were analyzed by flow cytometry (fluorescence-activated cell sorting, FACS). The Rh123 signal clearly decreased under laser plus SWNTs treatment (Figure 2B), thus indicating the decline of mitochondrial transmembrane potential ($\Delta\Psi$m) after treatment.

2.3. Photoacoustic Effect of SWNTs in vitro

To determine whether the photoacoustic effect of SWNTs could cause cell death through inducible mitochondrial explosion, we further detected the photoacoustic effect at the cellular level. First, we investigated the photoacoustic effect on cell viability with different energies of laser or different concentrations of SWNTs. The tumor cells were incubated with SWNTs for 2 h, followed by irradiation with a 1064 nm pulse laser. We found that treatment with laser energy of 17.5 mJ and a SWNT concentration of 10 μg mL^{-1} achieved significant cellular cytotoxicity (**Figure 3**Aa). The cellular cytotoxicity was obviously enhanced by the increase of SWNT concentrations from 2.5 to 20 μg mL^{-1} (Figure 3Ab). Apparently, the in vitro photoacoustic effect of SWNTs depends on both the SWNT concentration and the laser energy.

Furthermore, we investigated the *in situ* photoacoustic effect of SWNTs on mitochondria in intact tumor cells. EMT6 cells were stained with Rh123 and then incubated with SWNTs for 2 h before being irradiated by the 1064 nm pulse laser (17.5 mJ, 20 s). The changes in Rh123 fluorescence signal were analyzed by FACS. Under the laser treatment, the Rh123 signal decreased in the cells with concentrations of SWNTs from 5 to 20 μg mL^{-1} (Figure 3Ba). Notably, SWNTs of concentration 10 and 20 μg mL^{-1} caused nearly the same level of significant decrease in Rh123 signal compared with 5 μg mL^{-1} SWNTs (Figure 3Ba). Experiments using tetramethyl rhodamine methyl ester (TMRM), another $\Delta\Psi$m fluorescent probe, with confocal microscopy showed the same sharp decrease in $\Delta\Psi$m, which indicated the explosion of mitochondria (Figure 3Bb).

Release of cytochrome *c* is another indicator of mitochondria explosion. For cytochrome *c* release analysis, cells doubly expressing green fluorescent protein (GFP)-Cyt c and DsRed-mit were stimulated by various treatments. The fluorescence emission from GFP coincided with that of DsRed in control cells, thereby indicating the mitochondrial localization of cytochrome *c* under physiological conditions (Figure 3C). In contrast, in the laser plus SWNT-treated cells, the fluorescence emission from GFP diffused into the entire cell, clearly demonstrating the release of cytochrome *c* from mitochondria (Figure 3C). These results demonstrate that mitochondria-localized SWNTs can destroy the mitochondria under laser irradiation.

To clarify the cell death mode upon photoacoustic treatment, annexin V-FITC/propidium iodide (PI) double staining analysis was used. As expected, neither SWNTs nor laser treatment alone could induce cell death. In contrast, laser plus SWNTs treatment induced obvious cell death, revealed by the strong positive annexin V-FITC signal (Figure 3D). Statistical analysis of the data showed that laser plus SWNTs treatment induced 1.35% cell necrosis (PI positive cells),

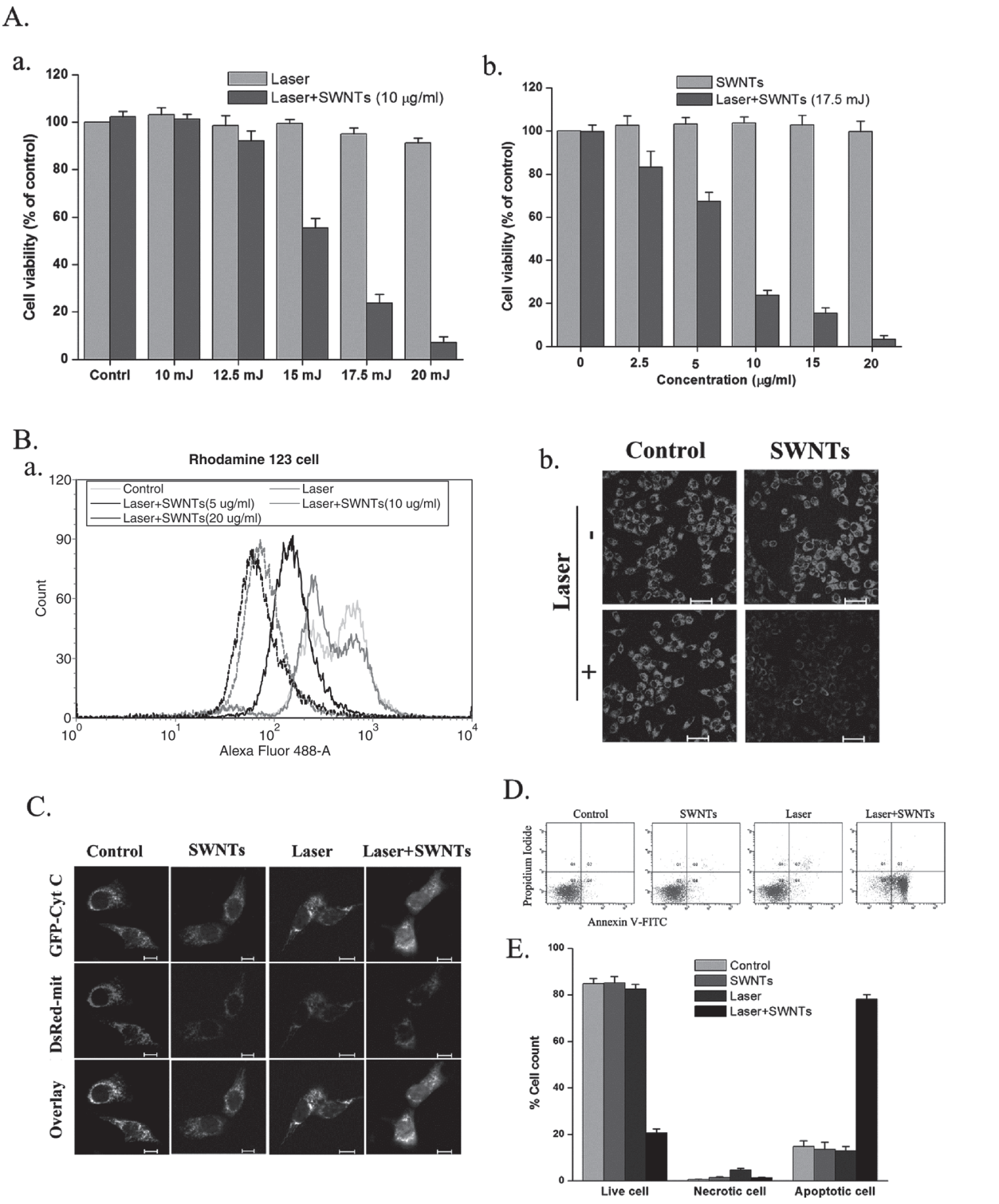

Figure 3. Photoacoustic effect of SWNTs on tumor cell death. A) Photoacoustic effect of SWNTs on cell viability under a) different energies of laser (10–20 mJ) or b) different concentrations of SWNTs (2.5–10 μg mL^{-1}). Cells were incubated with SWNTs for 30 min and then irradiated by a pulse laser. The treated cells were incubated in complete medium for 30 min before assessing cell viability. Cells without any treatment were used as control. Bars (means ± standard deviation, $n = 4$). B) Changes of $\Delta\Psi$m in mitochondria targeted by SWNTs. a) Rh123-stained cells were incubated with SWNTs (5–20 μg mL^{-1}) for 30 min with irradiation by a pulse laser (17.5 mJ for 20 s), then subjected to FACS analysis. The decrease in Rh123 signal represents the decline of $\Delta\Psi$m. b) TMRM-stained cells were incubated with SWNTs (10 μg mL^{-1}) for 30 min with irradiation by a pulse laser, then the fluorescence images were recorded by confocal microscopy. The disappearance of TMRM fluorescence represents the depolarization of mitochondria. C) Cytochrome *c* (Cyt c) release analysis. Cells expressing GFP-Cyt c and DsRed-mit were incubated with SWNTs (10 μg mL^{-1}) for 30 min before pulse laser irradiation (17.5 mJ for 20 s), then the fluorescence images were recorded by confocal microscopy. D,E) Cell death analysis. Cells were incubated with SWNTs (10 μg mL^{-1}) for 30 min before pulse laser irradiation (17.5 mJ for 20 s). Thirty minutes after treatment, the cells were subjected to cell death analysis by FACS with annexin V-FITC/PI double staining. All the data are representative of four independent experiments.

NANO MICRO small

and 79.4% cell apoptosis (annexin V-FITC positive cells; Figure 3E). Thus, these results show that the mechanism of in vitro photoacoustic therapy is cell apoptosis but not necrosis.

2.4. Photoacoustic Effect of SWNTs in vivo

The in vivo photoacoustic effect of SWNTs was evaluated using a mouse mammary tumor model. EMT6 cells were injected subcutaneously in the flank of female Balb/c mice. When the tumor size reached approximately 100 mm^3, the animals were divided into various treatment groups.

First, we investigated the mitochondrial localization of SWNTs in tumor tissue. Two hours after intratumoral injection with various reagents, mitochondria were separated from tumor tissue and then subjected to FACS analysis. With either FITC or PEG-FITC injection, the fluorescence emission from mitochondria remained nearly unchanged in comparison to the control group. In contrast, the fluorescence emission significantly increased with SWNT-PEG-FITC injection (**Figure 4**A). These results demonstrate the mitochondrial localization of SWNTs in tumor tissue.

Next, we explored whether SWNTs-based photoacoustic therapy could selectively destroy tumor tissue without damage to the epidermis. Figure 4B and C shows that after laser plus SWNTs treatment, almost all the cells isolated from the tumor tissue were dead whereas the epidermal cells were largely intact.

To determine tumor cytotoxicity of the photoacoustic effect with mitochondria-targeted SWNTs, scathe levels in tumors were examined 30 min after various treatments using hematoxylin and eosin (H&E) staining or terminal deoxynucleotidyl transferase dUTP nick end labeling (TUNEL) staining. Tumor cells treated by SWNTs alone or by laser alone showed similar levels of scathe compared to the untreated tumors (**Figure 5**A). In contrast, a high scathe level was observed in the cells treated by laser plus SWNTs (Figure 5A).

After treatment, the mice were observed daily and the tumor volumes were measured using a caliper every other day. The mice treated by laser only had an average tumor burden similar to that of untreated mice (Figure 5B). In contrast, laser plus SWNTs treatment significantly suppressed tumor growth and the suppression was positively correlated with the dose of SWNTs. Near total inhibition of tumor burden was found with SWNTs of dose 50 μg.

Next, we investigated whether tumor cytotoxicity was influenced by the photothermal effect during laser irradiation. Mice were treated by intratumoral injections of SWNTs (50 μg). Two hours post injection, the tumors were subjected to laser treatment at an energy of 17.5 mJ for 60 s. The spot size of the laser beam was adjusted to cover the entire tumor. During laser treatment, full-body thermographic images were captured using an infrared camera, as shown in Figure 5C. The temperature of the irradiated area was plotted as a function of the irradiation time (Figure 5D). For the SWNTs-injected mice, the tumor surface temperature increased only about 1 °C during laser treatment.

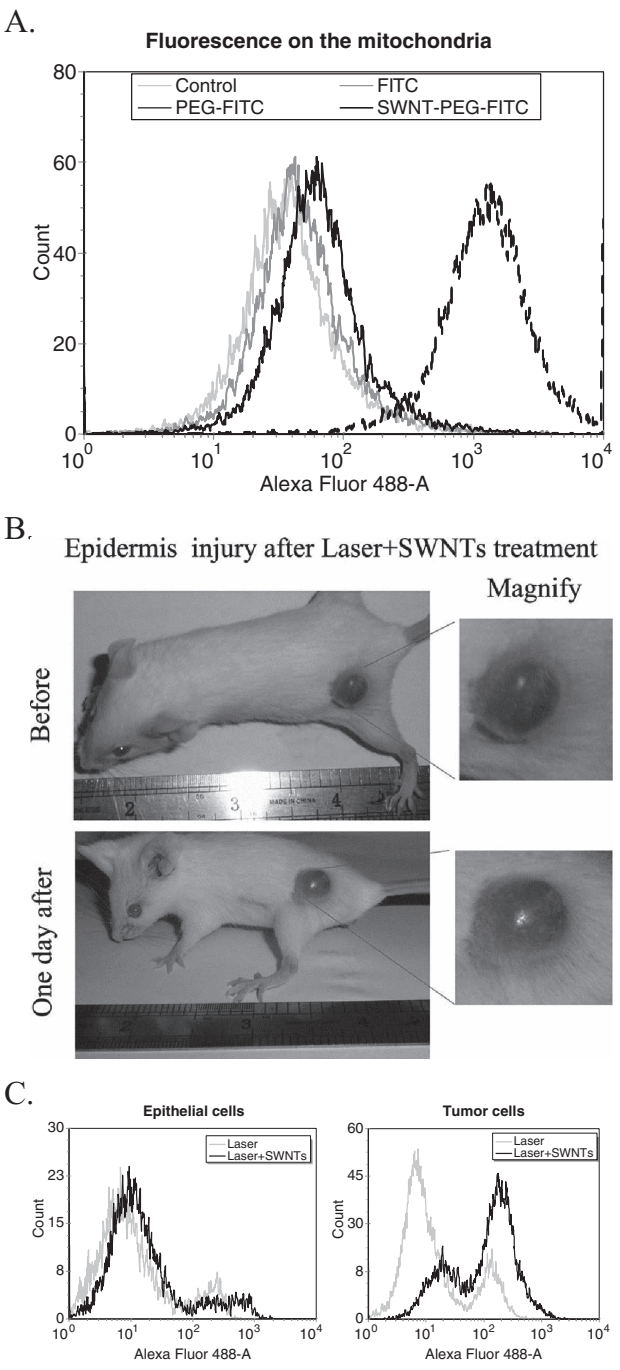

Figure 4. Tumor damage caused by photoacoustic therapy with mitochondria-targeted SWNTs. A) Mitochondrial localization of SWNTs in tumor tissue. Two hours after injection of various reagents into the center of the tumor tissue, mitochondria were separated from the tumor tissue and subjected to FACS analysis. A positive FITC signal was only detected in SWNT-PEG-FITC-injected tumors. B) Photographic images of epidermis injury on tumors after photoacoustic therapy. One day after laser treatment plus SWNTs injection, the epidermis injury of tumor tissues was observed, compared to SWNTs injection only. C) Cell apoptosis analysis using annexin V-FITC staining of tumor cells and epithelial cells after laser treatment with or without SWNTs injection. Upon laser treatment plus SWNTs injection, quite a low cell apoptosis rate was observed in epithelial cells in comparison to the high rate in tumor cells. All the data are representative of four independent experiments.

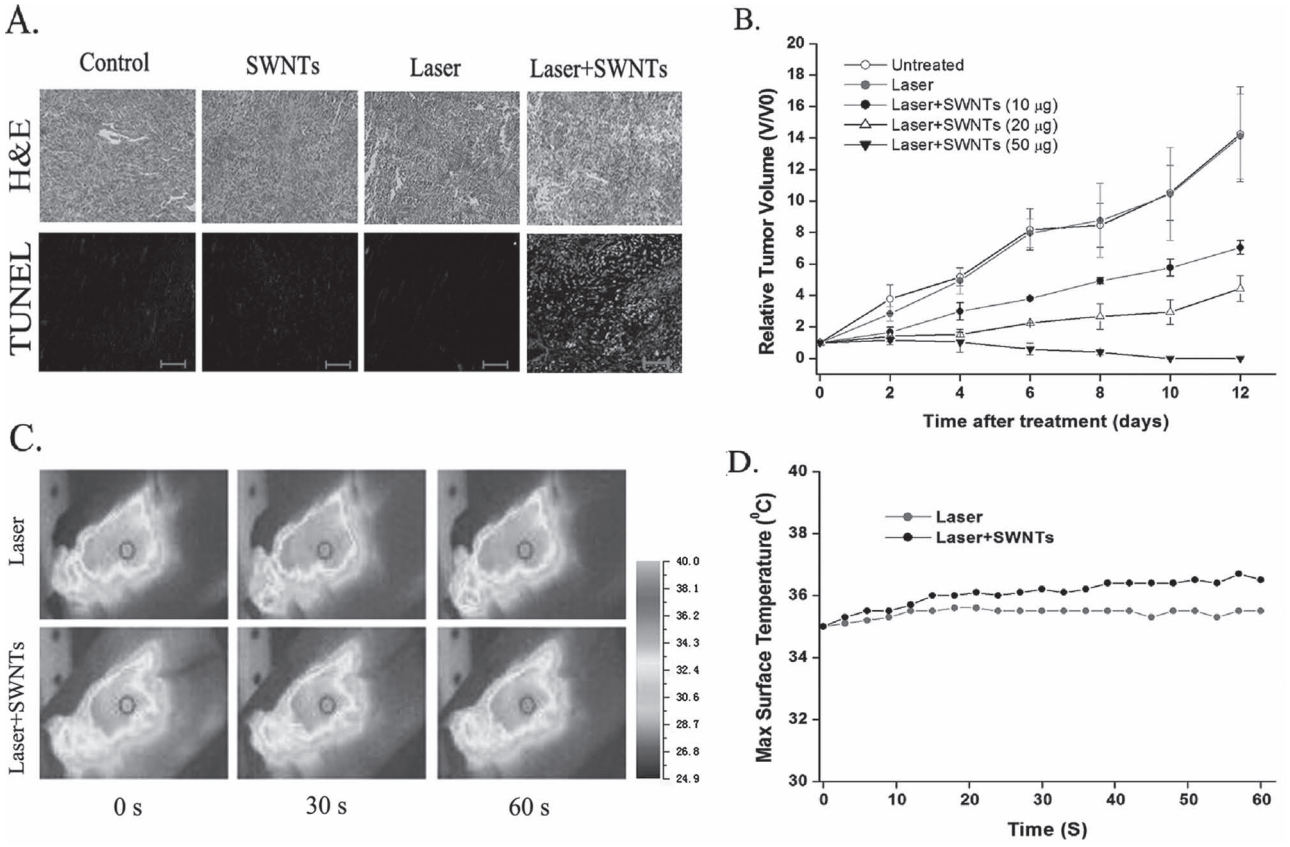

Figure 5. Photoacoustic effect of SWNTs on tumor therapy in vivo. A) Histological staining of the excised tumors 30 min after various treatments. The upper panel shows images with H&E staining of representative specimens at ×10 magnification. The lower panel shows images with TUNEL staining of representative specimens at ×40 magnification. High scathe level was only observed in the group that underwent laser treatment (17.5 mJ) plus SWNTs (50 μg) injection. B) Relative volumetric change in tumor size of various treatment groups. V0 was the tumor volume at the time of laser treatment. C,D) Monitoring of the changes in temperature on the surface of tumor tissue during laser treatment with or without SWNT injection. C) Thermographic images of the group that underwent laser treatment plus SWNTs injection versus laser treatment alone. D) Temperature changes on the indicated region in the left image. Only a small increase in temperature was observed in the group that underwent laser treatment (17.5 mJ) plus SWNTs (50 μg) injection. The results show the negligible thermal damage to the tumor surface caused by photoacoustic therapy with mitochondria-targeted SWNTs. All the data are representative of four independent experiments.

3. Discussion

Recently, the combination of nanomaterials and NIR light has provided a noninvasive, nontoxic, and selective therapeutic technique.[5,6,26–29] We chose a CoMoCAT nanotube suspension with PL-PEG in the present study since it exhibited a sharp absorption peak at 1016 nm (Figure 1A), thus meeting the requirements for selective phototherapy. The in vitro and in vivo effectiveness of photothermal therapy using a 980 nm continuous laser and CoMoCAT SWNTs has been demonstrated in our recently published work.[6,24,25] Herein, we developed a photoacoustic therapy for targeted cancer destruction by the large photoacoustic effect of SWNTs with the pulse laser. We confirmed that photoacoustic laser–tissue interaction using a pulse laser and SWNTs could be an effective local intervention due to the low light dose, noninvasiveness, and tumor targeting. It is clear from our data that the light energy can be transformed into sound energy by the SWNTs (Figure 1B), and this effect can be applied in photoacoustic imaging and photoacoustic therapy.

A previous study showed that PL-PEG-SWNT could localize in mitochondria. Herein, we confirmed the photoacoustic effect of SWNTs on single mitochondria during 1064 nm pulse laser irradiation. After incubation with SWNTs, laser irradiation could bomb the mitochondria into dysfunction (Figure 2B). The cellular cytotoxicity clearly depends on both the SWNT concentration and the laser dose (Figure 3A).

MOMP is an essential step for an intrinsic apoptosis pathway. Due to the permeabilization, some pro-apoptotic factors, such as cytochrome *c* in the mitochondrial intermembrane space, can be released into the cytosol, which in turn leads to activation of caspases, a family of proteases that act as common death effector molecules.[18–20] Compared to laser-only treatment, laser plus SWNTs treatment induced a much higher level of apoptotic cell death (Figure 3D

NANO MICRO small

and E) due to the dysfunction of mitochondria (Figure 3B and C). Therefore, we conclude that laser plus SWNTs photoacoustic therapy can initiate the mitochondrial pathway of apoptosis. In addition, our previous study found that apoptotic cell death afforded more tumor antigens and induced higher immune response during photodynamic therapy.[30] It is also reported that carbon nanotubes conjugated to tumor lysate protein could enhance the specific antitumor immune response.[31]

The use of mitochondria as therapeutic targets for cancer treatment has attracted much attention recently, because of the proliferative and bioenergetic difference between normal and cancerous cells.[21,23] Most cells derived from tumor mass had higher mitochondrial $\Delta\Psi m$ than normal epithelial cells.[22] Our previous study showed that the SWNTs could selectively accumulate in mitochondria due to the existence of $\Delta\Psi m$, with a higher level of accumulation in cancerous cells than normal cells.[24,25] Herein, our results showed that laser plus SWNTs could selectively destroy tumor tissue without epidermis injury (Figure 4). However, photothermal therapy with SWNTs could induce partial skin damage.[5] This difference between photothermal therapy and photoacoustic therapy is due to the different laser treatment model and laser dose. The photothermal effect results from continuous irradiation, with a higher laser dose in local tissue,[2,5,6] whereas the photoacoustic effect results from a pulsed light source causing transduction from light energy to acoustic pressure, with lower laser dose.[10,16]

With H&E and TUNEL staining analysis, a high scathe level was observed in the laser plus SWNTs treated tumors (Figure 5A). The enhanced tumor-killing effect was due to the fact that SWNTs can selectively absorb the 1064 nm laser light, transduce to acoustic pressure, and bomb the mitochondria.

Laser plus SWNTs treatment caused significant tumor suppression (Figure 5B). With increasing concentrations of SWNTs, remarkable enhancement of photoacoustic destruction of tumor cells can be observed (Figure 5B). The skin overlying the mouse tumor experienced only a small temperature increase (Figure 5C and D), which is entirely different from past photothermal techniques that heat the SWNTs in tumor tissue to high temperature.[5,6]

4. Conclusion

We have presented a new photoacoustic therapy model for cancer treatment using mitochondria-targeted SWNTs. The SWNTs can be more efficiently accumulated in mitochondria of cancerous cells due to the high $\Delta\Psi m$ compared with that of normal cells. Upon NIR pulse laser treatment, cancer-cell mitochondria can be destroyed directly by the photoacoustic effect of SWNTs. Minimal normal cell damage and reduced laser dose can be achieved because of the high-level accumulation of SWNTs in mitochondria of cancer cells. Therefore, the combination of laser and SWNTs could prove to be a promising mitochondria-targeting photoacoustic therapy for cancer treatment.

5. Experimental Section

Functionalization of SWNTs: Functionalization of SWNTs with PL-PEG-NH_2 or FITC was performed following the procedures previously described.[24,25] Briefly, CoMoCAT SWNTs[32] with an average diameter of 0.81 nm and length 500–1500 nm were sonicated in an aqueous solution of PL-PEG-NH_2 (1 mg SWNTs, 1 mg PL-PEG, 1 mL water) for 6 h. The mixture was then centrifuged at 10 000 *g* for 15 min, and the supernatant was collected. Excess phospholipids were removed by repeated filtration using 100 kDa filters (Millipore Corporation, Billerica, MA) and rinsing with phosphate-buffered saline (PBS).

FITC (1 mM) was mixed with SWNT-PL-PEG-NH_2 solution (1 mL) overnight at room temperature, avoiding light exposure. The SWNT-PL-PEG-FITC was filtered through 100 kDa filters (Millipore Corporation, Billerica, MA) to remove excess FITC.

Optical Spectroscopy: The optical absorbance of SWNTs was measured using a UV/Vis–NIR spectrometer (Lambda 35, Perkin–Elmer, USA). Raman spectra were measured with a microscopic Raman spectrometer (Nippon Optical System Co., Japan). The excitation source was from a He–Ne laser (Melles Griot, USA) tuned at 632.8 nm with a power of 2 mW at the sample location. The typical accumulation time used in this study was 20 s.

Photoacoustic Therapy: A Nd:YAG (neodymium-doped yttrium aluminum garnet) laser (Brilliant B, Bigsky) with wavelength of 1064 nm, output of 8 ns pulse width, and repetition rate of 10 Hz was used to irradiate the targets; the laser was transmitted with an optical fiber. The experiments were conducted with an energy density of 10–20 mJ cm^{-2}.

Temperature Measurement during NIR Radiation: For ex vitro experiments, SWNT solutions were irradiated by the Nd:YAG pulse laser for 30 s, and the temperature was measured in 3 s intervals with an infrared thermal camera (TVS200EX, NEC, Japan). For in vivo measurement, tumors injected with different samples were irradiated by the pulse laser for 60 s, and the surface temperatures of the tumors were measured in 3 s intervals with the infrared thermal camera. All the experiments were conducted at room temperature.

Cell Culture and Transfection: Mouse mammary tumor cell line EMT6 was used in this study. Cells were cultured in RPMI 1640 (GIBCO, Grand Island, NY), supplemented with 15% fetal calf serum (FCS), penicillin (100 units mL^{-1}), and streptomycin (100 μg mL^{-1}) in 5% CO_2, 95% air at 37 °C in a humidified incubator. Cells cultured on the glass microscopy coverslips were transfected with plasmid DNA (1 μg) of CFP-lamp, GFP-Cyt c, or DsRed-mit in the transfection solution at 37 °C for 4 h, then cultured in RPMI 1640 for 24 h before experiments.

Confocal Laser Scanning Microscopy: Fluorescence emissions from FITC (Sigma, St Louis, MO), MitoTracker Red (100 nM, Invitrogen Life Technologies, Inc., Carlsbad, CA), CFP, DsRed, GFP, and TMRM were observed confocally using a commercial laser scanning microscope (LSM 510 META) combination system (Zeiss, Jena, Germany) equipped with a Plan-Neofluar 40×/1.3 numerical aperture (NA) oil DIC objective. Excitation wavelength and detection filter settings for each of the fluorescent indicators were as follows. FITC and GFP were excited at 488 nm with an argon-ion laser (reflected by a beam splitter HFT 488 nm), and the fluorescence emission was recorded through a 500–530 nm IR band-pass filter. CFP was excited at 458 nm with an argon-ion laser, and emitted light was recorded through a 470–500 nm IR band-pass filter. MitoTracker Red was excited at 633 nm with a He–Ne laser,

and emitted light was recorded through a 650 nm long-pass filter. DsRed and TMRM were excited at 543 nm with a He–Ne laser, and emitted light was recorded through a 600 nm long-pass filter.

Detection of Mitochondrial Potential Depolarization: TMRM (100 nM, Molecular Probes, Inc., Eugene, OR) and Rh123 (5 μM, Sigma–Aldrich, St Louis, MO) were used as an indicator of mitochondrial depolarization. Cells (1×10^4 per well) growing in 35-mm Petri dishes were stained with TMRM or Rh123 for 20 min at 37 °C, and rinsed three times with PBS prior to fluorescence measurement by confocal microscopy or FACS.

Cell Apoptosis Detection: Tumor cells were harvested 30 min after treatment, stained with annexin V-FITC and PI (BD PharMingen, Mountain View, CA), and analyzed by flow cytometry (FACScanto II, BD Bioscience, Mountain View, CA) with excitation at 488 nm. The fluorescence emission of FITC was measured at 515–545 nm and that of DNA–PI complexes at 564–606 nm. Compensation was used wherever necessary.

Animal Models: EMT6 cells (1×10^6) in solution (100 μL) were injected into the flank region of female Balb/c mice, aged 6–8 weeks. Animals were used in experiments 5 days after tumor-cell inoculation when the tumors reached a size of approximately 100 mm^3.

Cell Death Assays: Cytotoxicity in vitro was examined with a colorimetric tetrazolium salt-based assay using a Cell Counting Kit-8 (CCK8, Dojindo Laboratories, Kumamoto, Japan) as described previously.[33] To detect cytotoxicity, tumor cells were irradiated by the pulse laser at an energy of 10–20 J cm^{-2} with or without SWNTs incubation. OD450, the absorbance value at 450 nm, was read with a 96-well plate reader (INFINITE M200, Tecan, Switzerland) to determine the viability of the cells.

For cell death analysis in vivo, the tumors were harvested 30 min after treatment. Individual tumors were fixed in 10% neutral buffered formalin, processed routinely into paraffin, sectioned at 5 μm, stained with H&E or TUNEL fluorescent dye (Genmed, Boston, MA), and examined by optical or fluorescence microscopy.

Statistics: Each experiment was performed at least three times. Statistical analysis was applied using the two-tailed Student's *t* test. Otherwise, representative data are shown.

Acknowledgements

This research was supported by the National Basic Research Program of China (2011CB910402; 2010CB732602), the Program for Changjiang Scholars and Innovative Research Team in University (IRT0829), and the National Natural Science Foundation of China (30870676; 81101741), Science and Technology Planning Project of Guangdong Province (2011B031300008). The authors thank Professor Daniel E. Resasco of the University of Oklahoma for providing CoMoCAT SWNTs, Y. Gotoh (Institute of Molecular and Cellular Bioscience, University of Tokyo) for providing pDsRed-mit, and Dr. G. J. Gores (Center for Basic Research in Digestive Diseases, Molecular Medicine Program, Mayo Clinic, Rochester, MN, USA) for providing the pCyt c-GFP plasmid.

[1] M. J. O'Connell, S. M. Bachilo, C. B. Huffman, V. C. Moore, M. S. Strano, E. H. Haroz, K. L. Rialon, P. J. Boul, W. H. Noon, C. Kittrell, *Science* **2002**, *297*, 593.
[2] N. W. S. Kam, M. J. O'Connell, J. A. Wisdom, H. Dai, *Proc. Natl. Acad. Sci. USA* **2005**, *102*, 11600.
[3] K. König, *J. Microsc. (Oxford)* **2000**, *200*, 83.
[4] R. Weisslder, *Nat. Biotechnol.* **2001**, *19*, 316.
[5] H. K. Moon, S. H. Lee, H. C. Choi, *ACS Nano* **2009**, *3*, 3707.
[6] F. Zhou, D. Xing, Z. Ou, B. Wu, D. E. Resasco, W. R. Chen, *J. Biomed. Opt.* **2009**, *14*, 021009.
[7] P. M. Ajayan, M. Terrones, A. de la Guardia, V. Huc, N. Grobert, B. Q. Wei, H. Lezec, G. Ramanath, T. W. Ebbesen, *Science* **2002**, *296*, 705.
[8] S. H. Tseng, N. H. Tai, W. K. Hsu, L. J. Chen, J. H. Wang, C. C. Chiu, C. Y. Lee, L. J. Chou, K. C. Leou, *Carbon* **2007**, *45*, 958.
[9] B. Bockrath, J. K. Johnson, D. S. Sholl, B. Howard, C. Matranga, W. Shi, D. Sorescu, *Science* **2002**, *297*, 192.
[10] B. Kang, D. Yu, Y. Dai, S. Chang, D. Chen, Y. Ding, *Small* **2009**, *5*, 1292.
[11] A. de la Zerda, C. Zavaleta, S. Kere, S. Vaithilingam, S. Bodapati, Z. Liu, J. Levi, B. R. Smith, T. J. Ma, O. Oralkan, Z. Cheng, X. Chen, H. Dai, B. T. Khuri-Yakub, S. S. Gambhir, *Nat. Nanotechnol.* **2008**, *3*, 557.
[12] M. Pramanik, K. H. Song, M. Swierczewska, D. Green, B. Sitharaman, L. V. Wang, *Phys. Med. Biol.* **2009**, *54*, 3291.
[13] M. Pramanik, M. Swierczewska, D. Green, B. Sitharaman, L. V. Wang, *J. Biomed. Opt.* **2009**, *14*, 034018.
[14] L. Xiang, Y. Yuan, D. Xing, Z. Ou, S. Yang, F. Zhou, *J. Biomed. Opt.* **2009**, *14*, 021008.
[15] C. Kim, C. Favazza, L. V. Wang, *Chem. Rev.* **2010**, *110*, 2756.
[16] B. Kang, Y. Dai, S. Chang, D. Chen, *Carbon* **2008**, *46*, 978.
[17] A. S. Don, P. J. Hogg, *Trends Mol. Med.* **2004**, *10*, 372.
[18] C. Wang, R. J. Youle, *Annu. Rev. Genet.* **2009**, *43*, 95.
[19] S. Desagher, J. C. Martinou, *Trends Cell Biol.* **2000**, *10*, 369.
[20] S. W. G. Tait, D. R. Green, *Nat. Rev.* **2010**, *11*, 621.
[21] V. Gogvadze, S. Orrenius, B. Zhivotovsky, *Trends Cell Biol.* **2008**, *18*, 165.
[22] L. B. Chen, *Annu. Rev. Cell Biol.* **1988**, *4*, 155.
[23] S. Fulda, L. Galluzzi, G. Kroemer, *Nat. Rev.* **2010**, *9*, 447.
[24] F. Zhou, D. Xing, B. Wu, S. Wu, Z. Ou, W. R. Chen, *Nano Lett.* **2010**, *10*, 1677.
[25] F. Zhou, S. Wu, B. Wu, W. R. Chen, D. Xing, *Small* **2011**, *7*, 2727.
[26] L. R. Hirsch, R. J. Stafford, J. A. Bankson, S. R. Sershen, B. Rivera, R. E. Rrice, J. D. Hazle, N. J. Halas, J. L. West, *Proc. Natl. Acad. Sci. USA* **2003**, *100*, 13549.
[27] J. Chen, C. Glaus, R. Laforest, Q. Zhang, M. Yang, M. Gidding, M. J. Welch, Y. Xia, *Small* **2010**, *6*, 811.
[28] A. Burke, X. Ding, R. Singh, R. A. Kraft, N. L. Poluachenko, M. N. Rylander, C. Szot, C. Buchanan, J. Whitney, J. Fisher, H. C. Hatcher, R. D'Agostino, N. D. Kock, P. M. Ajayan, D. L. Carroll, S. Akman, F. M. Torti, S. V. Torti, *Proc. Natl. Acad. Sci. USA* **2009**, *106*, 12897.
[29] K. Yang, S. Zhang, G. Zhang, X. Sun, S. T. Lee, Z. Liu, *Nano Lett.* **2010**, *10*, 3318.
[30] F. Zhou, D. Xing, W. R. Chen, *Int. J. Cancer* **2009**, *125*, 1380.
[31] J. Meng, J. Duan, H. Kong, L. Li, C. Wang, S. Xie, S. Chen, N. Gu, H. Xu, X. D. Yang, *Small* **2008**, *4*, 1364.
[32] S. M. Bachilo, L. Balzano, J. E. Herrera, F. Pompeo, D. E. Resasco, R. B. Weisman, *J. Am. Chem. Soc.* **2003**, *125*, 11186.
[33] F. Zhou, D. Xing, W. R. Chen, *Cancer Lett.* **2008**, *264*, 135.

Received: September 12, 2011
Revised: December 13, 2011
Published online: March 16, 2012

